iScience

CellPress
OPEN ACCESS

Article

Pathogenic mycobacterium upregulates cholesterol 25-hydroxylase to promote granuloma development via foam cell formation

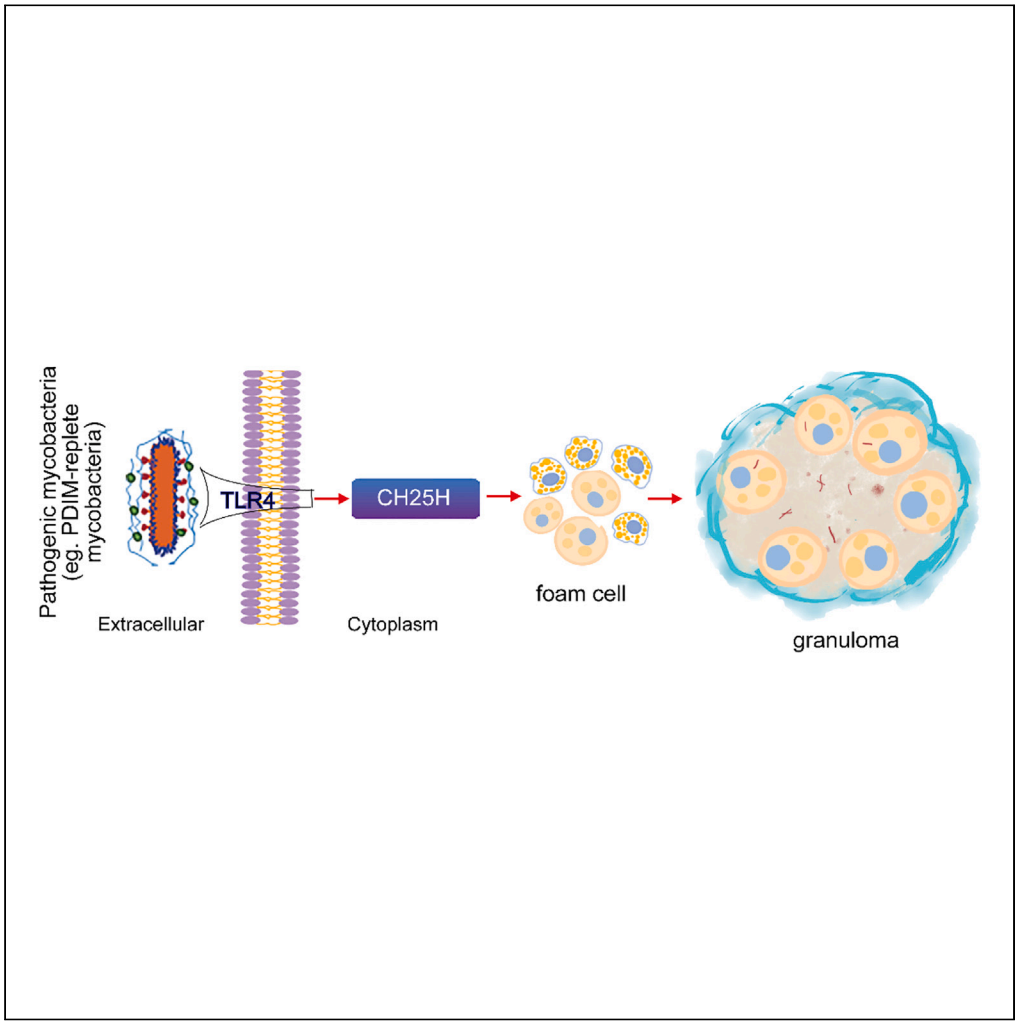

Shuang Zhou, Ding Zhang, Dan Li, ..., Laura E. Via, Lu Zhang, Decheng Wang

zhanglu407@fudan.edu.cn (L.Z.)
dcwang99@163.com (D.W.)

Highlights

CH25H was induced and upregulated in pathogenic mycobacteria-infected macrophages

CH25H was a critical factor in modulating foam cell formation and expressed in granuloma

CH25H-*null* mice showed reduced foam cell formation and pathology upon *Mm* infection

CH25H may act as a player during statins-mediated adjuvant therapy against tuberculosis

Zhou et al., iScience *27*, 109204
March 15, 2024
https://doi.org/10.1016/j.isci.2024.109204

iScience

CellPress
OPEN ACCESS

Article

Pathogenic mycobacterium upregulates cholesterol 25-hydroxylase to promote granuloma development via foam cell formation

Shuang Zhou,[1,7,8] Ding Zhang,[1,8] Dan Li,[2,8] Hankun Wang,[1,8] Cairong Ding,[1] Jingrui Song,[1] Weifeng Huang,[1] Xuan Xia,[1] Ziwei Zhou,[3] Shanshan Han,[1] Zhu Jin,[2] Bo Yan,[4] Jacqueline Gonzales,[5] Laura E. Via,[5,6] Lu Zhang,[3,*] and Decheng Wang[1,9,*]

SUMMARY

Pathogenic mycobacteria orchestrate the complex cell populations known as granuloma that is the hallmark of tuberculosis. Foam cells, a lipid-rich cell-type, are considered critical for granuloma formation; however, the causative factor in foam cell formation remains unclear. Atherosclerosis is a chronic inflammatory disease characterized by the abundant accumulation of lipid-laden-macrophage-derived foam cells during which cholesterol 25-hydroxylase (CH25H) is crucial in foam cell formation. Here, we show that *M. marinum* (*Mm*), a relative of *M. tuberculosis*, induces foam cell formation, leading to granuloma development following CH25H upregulation. Moreover, the *Mm*-driven increase in CH25H expression is associated with the presence of phthiocerol dimycocerosate, a determinant for *Mm* virulence and integrity. CH25H-*null* mice showed decreased foam cell formation and attenuated pathology. Atorvastatin, a recommended first-line lipid-lowering drug, promoted the elimination of *M. marinum* and concomitantly reduced CH25H production. These results define a previously unknown role for CH25H in controlling macrophage-derived foam cell formation and Tuberculosis pathology.

INTRODUCTION

Tuberculosis, caused by *Mycobacterium tuberculosis* (*Mtb*), is the leading global cause of death from a bacterial infectious disease. As an intracellular bacterium, *Mtb* has developed numerous strategies to adapt to the host's internal microenvironment to benefit its survival.[1,2] Phthiocerol dimycocerosates (PDIM), an outer mycomembrane lipid of the cell wall, is ubiquitously distributed in all clinically and veterinary pathogenic mycobacterial species.[3–5] *Mycobacterium marinum* (*Mm*), a close relative of *Mtb* that shares most evolutionary homologous genes and common virulence determinants,[6] has been widely used to model the pathogenesis and underlying mechanisms of host-*Mtb* interactions.[7–9] Importantly, *Mm* can establish infection in a murine model via intravenous inoculation and form granulomatous lesions, providing scope for new avenues of study to reveal fundamental mechanisms of mycobacterial pathogenesis.[10]

Granuloma, a hallmark of tuberculosis, is an architecture of various cell types and is traditionally considered necessary for restraining mycobacterial dissemination[11,12]; however, the significance of granuloma for tuberculosis has gradually changed with accumulating reports.[7,11–13] Many studies have demonstrated that granulomas do not simply contain the bacilli but provide mycobacteria with a nutrient pool for survival.[7,11–14] Foam cells, lipid-laden macrophages that ubiquitously express adipocyte differentiation-related protein (ADRP), were originally described in atherosclerosis,[15,16] a condition that also forms during mycobacterial infection.[14,17–21] Macrophage-derived foam cells with accumulated lipids provide a hospitable parasitic microenvironment and act as a reservoir for live *Mtb* within the host.[21] Peroxisome proliferator-activated receptor gamma (PPARγ) is triggered by mycobacterial infection, leading to lipid droplet formation and reduced macrophage

[1]Hubei Key Laboratory of Tumor Microenvironment and Immunotherapy, China Three Gorges University; Institute of Infection and Inflammation, China Three Gorges University; College of Basic Medical Sciences, China Three Gorges University, Yichang 443002, P.R. China
[2]Department of Tuberculosis, The Third People's Hospital of Yichang, Yichang 443003, P.R. China
[3]State Key Laboratory of Genetic Engineering, Institute of Genetics, MOE Engineering Research Center of Gene Technology, School of Life Science, Fudan University, Shanghai 200433, P.R. China
[4]Shanghai Public Health Clinical Center, Fudan University, Shanghai China
[5]Tuberculosis Research Section, Laboratory of Clinical Infectious Diseases, Division of Intramural Research, National Institute of Allergy and Infectious Diseases, National Institutes of Health, Bethesda, MD 20982, USA
[6]Institute of Infectious Disease and Molecular Medicine, University of Cape Town, Cape Town, South Africa
[7]Present address: Wuhan Jinyintan Hospital, Tongji Medical College of Huazhong University of Science and Technology ; Hubei Clinical Research Center for Infectious Diseases ; Wuhan Research Center for Communicable Disease Diagnosis and Treatment, Chinese Academy of Medical Sciences ; Joint Laboratory of Infectious Diseases and Health, Wuhan Institute of Virology and Wuhan Jinyintan Hospital, Chinese Academy of Sciences, Wuhan, 430023, China
[8]These authors contribute equally
[9]Lead contact
*Correspondence: zhanglu407@fudan.edu.cn (L.Z.), dcwang99@163.com (D.W.)
https://doi.org/10.1016/j.isci.2024.109204

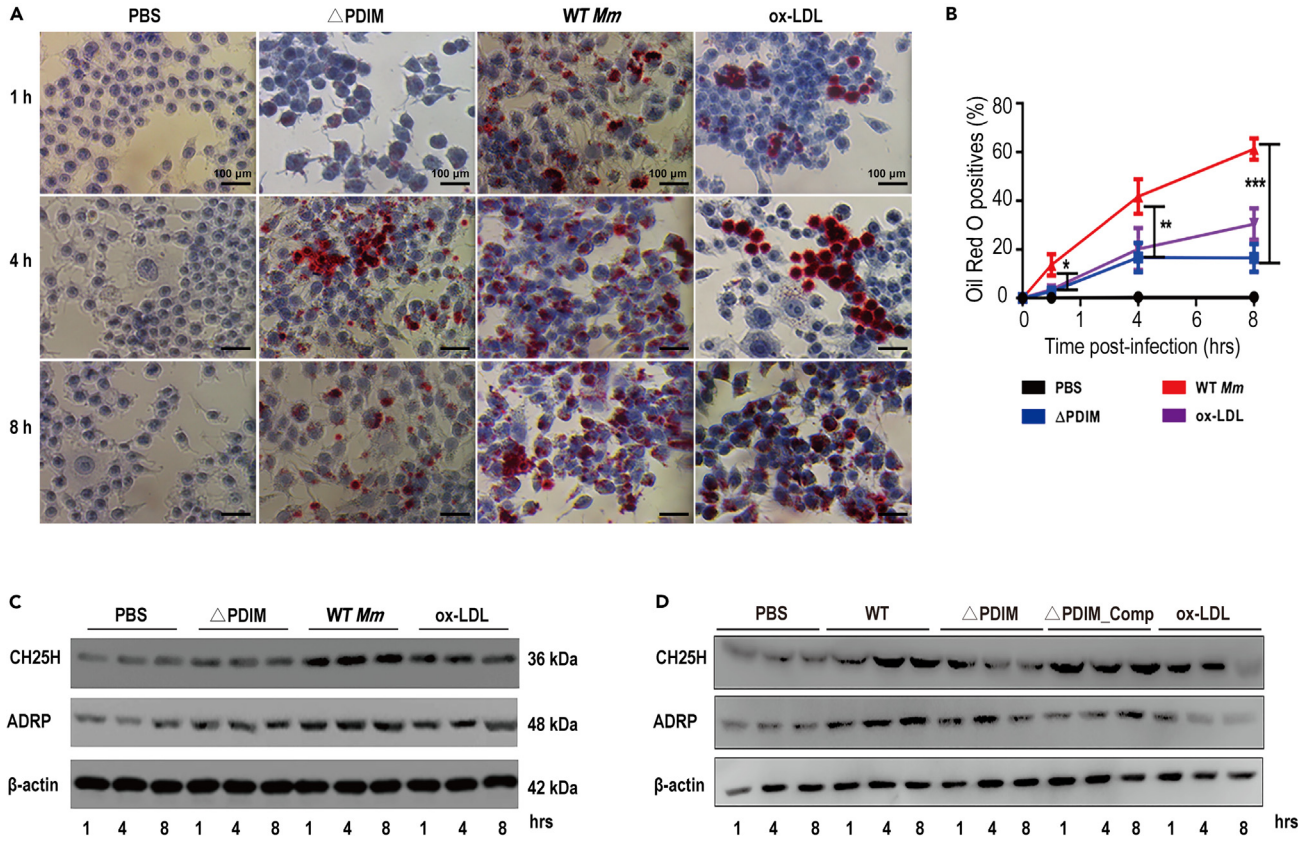

Figure 1. Pathogenic mycobacteria induce foam cell formation and CH25H upregulation

(A) In *Mm*-infected Raw264.7 macrophages (MOI = 5), wide-type (WT) *Mycobacterium marinum* (*Mm*) induced most of macrophages transdifferentiation into foam cells compared with a cell wall lipid PDIM mutant (ΔPDIM) at 1, 4, and 8 hpi. ox-LDL (50 μg/mL) treatment as a positive control (40× magnification).

(B) Quantitation of foam cell density demonstrated a significant difference between WT_*Mm* and ΔPDIM-treated groups at 1, 4, and 8 hpi (*$p < 0.05$, **$p < 0.01$, ****$p < 0.0001$). Data are representative of three biologically independent experiments.

(C) The cell lysates of WT_ *Mm* and/or ΔPDIM-treated cells were prepared and analyzed by western blot and demonstrated that CH25H was upregulated transparently in WT_*Mm*-infected Raw264.7 cells, while weakly expressed in ΔPDIM strain-challenged groups at matched time-points. Moreover, ADRP—a specific marker for foam cells, consistent with the CH25H expression at matched time-points between WT_*Mm* and ΔPDIM strain.

(D) Western blot detection demonstrated that complementation of ΔPDIM strain (ΔPDIM_Comp) restores the expression of CH25H and ADRP.

responses.[17,18] CD36 plays a role in the formation of foam macrophages and provides a protective niche for mycobacteria,[19] while targeting CD36 curtails *Mtb* survival by repressing foam cell formation.[22] In *Mm*-infected zebrafish, foam cells are converted from macrophages and their formation is driven by the mycobacterial ESX1 locus.[23] Recently, studies have revealed that lipid-lowering statin drugs inhibit foam cell formation and synergistically promote antimicrobial effects of tuberculosis treatments such as rifampicin and isoniazid *in vivo* and *in vitro*.[24–26] Although cumulative evidence demonstrates that statins have potential as anti-tuberculosis therapeutics, how statins manipulate foam cell development and the underlying mechanism requires further investigation.

Cholesterol 25-hydroxylase (CH25H), which hydroxylates cholesterol to generate 25-hydroxycholesterol (25HC)[27] and is highly expressed in activated macrophages[28] as well as the lungs of mice from an *Mtb* aerosol-infected model,[29] has been demonstrated to have not only broad antiviral activity,[28,30] but also play a critical role in modulating inflammatory responses.[31,32] Particularly, CH25H was proven to be a pivotal player in promoting macrophage differentiation into foam cells, mediating the accumulation of lipid droplets in macrophages to trigger the onset of atherogenesis.[16,32,33] However, to our knowledge, no reports have investigated the significance and mechanism of CH25H on foam cell formation during mycobacterial infection.

Here, we show that *M. marinum* (*Mm*), manipulates foam cell development via CH25H induction. Moreover, increased CH25H expression in *Mm*-infected cells was induced by PDIM, a virulence determinant present in *Mm*.[34,35] Knock-out of CH25H decreased foam cell formation and significantly attenuated pathology in *Mm*-infected mice. Atorvastatin, a recommended first-line statin, promoted the elimination of *Mm* *in vivo* and *in vitro* by reducing CH25H. Taken together, these results define a previously unknown role for CH25H in controlling macrophage-derived foam cell formation and tuberculosis pathology, demonstrating that CH25H-targeting may represent a promising adjuvant strategy for tuberculosis therapy in the future.

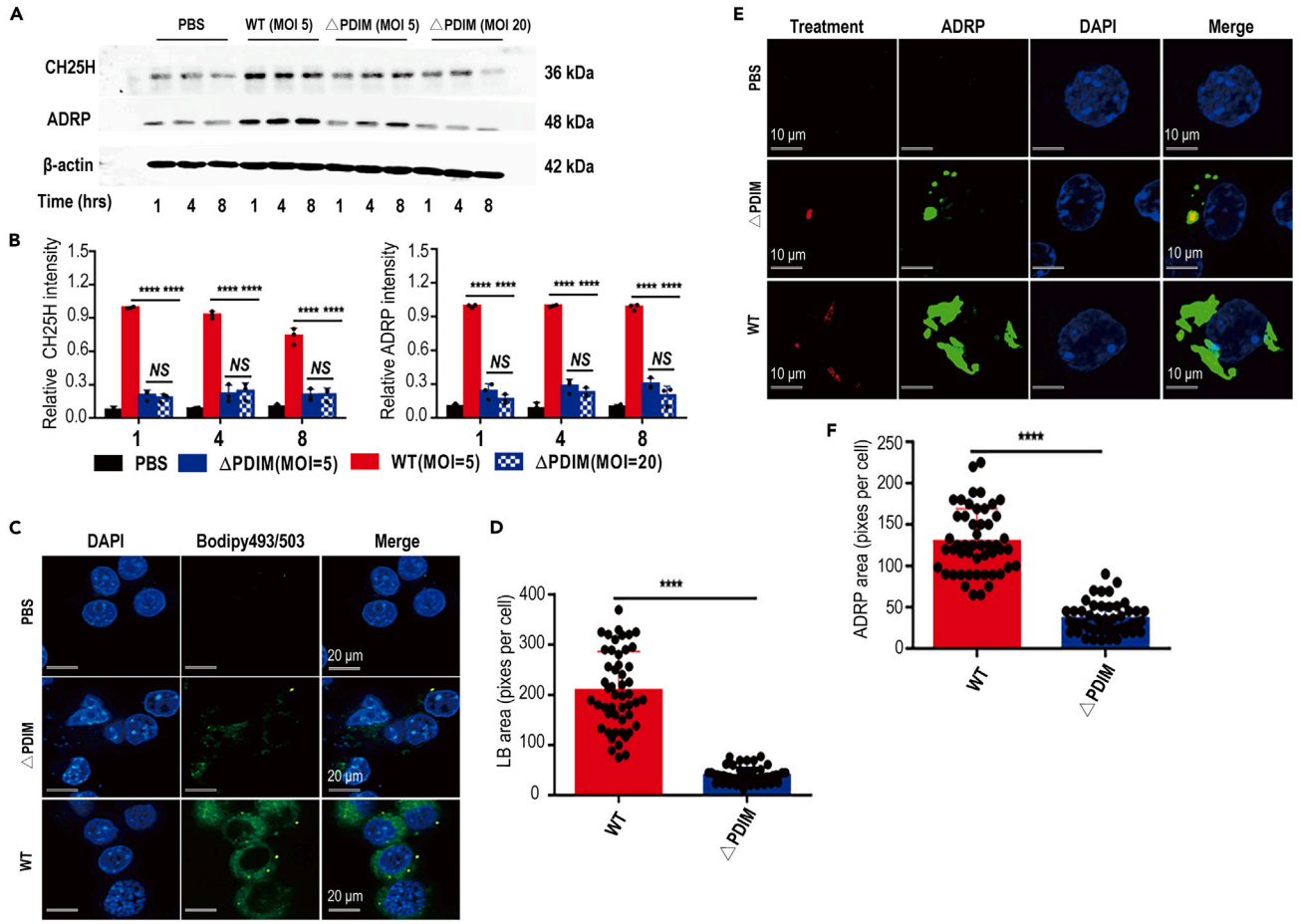

Figure 2. Pathogenic mycobacteria induce CH25H expression via a virulence-determinant-dependent manner

(A and B) At MOI = 5, WT_*Mm* induced abundant CH25H and ADRP proteins compared with those in ΔPDIM-treated cells. While enhancing the ΔPDIM MOI at 20, the protein levels of CH25H and ADRP were still lower and equivalent to ΔPDIM MOI = 5 at indicated time-points (****$p < 0.0001$). Data are representative of three biologically independent experiments.

(C and D) WT_*Mm* and ΔPDIM strain treated Raw264.7 macrophages for 4 h, stained for neutral lipids (BODIPY 493/503×) (C, 40× magnification) and quantitation between WT_ *Mm* and ΔPDIM treated groups, respectively (****$p < 0.0001$). Data are representative of three biologically independent experiments.

(E and F) Fluorescent images show *M. marinum* (red), nuclear fluorescence (DAPI, blue), ADRP (green) and stained for the foam cell marker ADRP (merged) ((E): 100× magnification). Quantitation for ADRP at 4 hpi between WT- and ΔPDIM *Mm*-treated groups (****$p < 0.0001$). Data are representative of three biologically independent experiments.

RESULTS

WT_*Mm* induced foam cell formation and CH25H induction

Numerous foam cells were formed in the WT_*Mm*-challenged group at 1, 4, and 8 hpi, whereas this was dramatically decreased in the ΔPDIM-infected group (Figure 1A). Quantitation showed that WT_*Mm* indeed induced significantly more foam cells compared with ΔPDIM (*$p < 0.05$; **$p < 0.01$; ***$p < 0.001$) (Figure 1B). Subsequently, western blot revealed that CH25H was significantly upregulated in the WT_*Mm*-infected group compared with ΔPDIM-infected cells (Figures 1C and S1A). ADRP, the hallmark of foam cells, was also clearly increased in the WT_*Mm*-infected group, while reduced in ΔPDIM-challenged cells (Figures 1C and S1B). CH25H and 25HC were markedly upregulated in WT_*Mm*-infected macrophages (Figures 1C, S1C and S1D); however, they did not show significant changes in the ΔPDIM-infected groups (Figures 1C, S1C, and S1D). Moreover, the complementation of ΔPDIM mutant (ΔPDIM_Comp) not only restored the expression of CH25H and ADRP (Figures 1D and S1E–S1H), but also enhanced the formation of foam cells (Figures S1I and S1J). Collectively, these results suggest that pathogenic mycobacteria promote foam cell formation and CH25H expression.

PDIM-replete mycobacteria upregulate CH25H expression during mycobacterial infection

PDIM-deficiency has been shown to decrease the uptake of mycobacteria by macrophages.[36] Consistent with this previous report, we found fewer ΔPDIM bacteria were taken up by macrophages compared with the WT_*Mm* at a multiplicity of infection (MOI) 5 (Figure 2S). To exclude

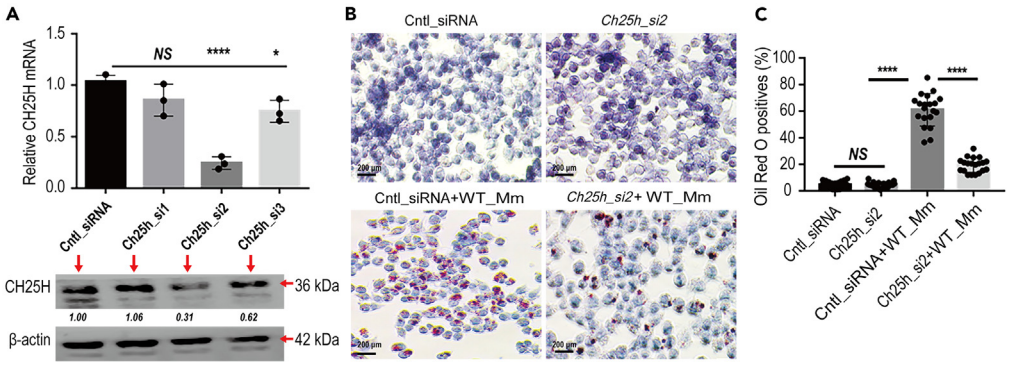

Figure 3. Silencing CH25H reduces the foam cell formation after WT_*Mm* infection

(A) Three siRNAs targeting the mouse *Ch25h* gene were designed and their efficiency was examined and demonstrated that siRNA-2 has an optimal inhibitory effect on the mouse *Ch25h* gene (termed as *Ch25h*_si2), which has been chosen for the continuous experiment.

(B) *Ch25h*_si2 was transfected into Raw264.7 cells and subsequently challenged with WT_*Mm*, then the cells were harvested and performed Oil Red O staining (40× magnification).

(C) Quantitation demonstrated that there was a significant difference with CH25H silencing in the WT_ *Mm*-infected group compared with without CH25H inhibition (****p < 0.0001; *NS*, no significance). Data are representative of three biologically independent experiments.

the possibility that decreased CH25H production was a result of fewer internalized ΔPDIM_*Mm* at MOI 5, we set up another group of ΔPDIM infections at MOI 20 to ensure intracellular mycobacteria numbers were equal to those occurring in WT_*Mm* infections at MOI 5. Despite the internalized bacteria in the ΔPDIM_*Mm*-infected group at MOI 20 being equivalent to WT_*Mm* infection at MOI 5 (Figure 2S), surprisingly, CH25H protein in the ΔPDIM group remained lower than that in WT_*Mm*-infected macrophages at MOI 5 (Figures 2A and 2B). Consistently, the foam cell marker ADRP was dramatically upregulated in the WT_*Mm*-infected group, but expressed at lower levels in macrophages infected with ΔPDIM at MOI 5 and 20 (Figures 2A and 2B). Staining for neutral lipids (Figures 2C and 2D) and immunofluorescence observation found that more lipid droplets and high expression of ADRP occurred in the WT_*Mm*-infected group (Figures 2E and 2F). These results indicate that mycobacteria replete with PDIM on their surface are required for the enhancement of expression of CH25H and ADRP during WT_*Mm* infection.

CH25H contributes to foam cell formation

To assess whether CH25H contributes to foam cell formation upon WT_*Mm* infection, specific small interfering (si) RNAs against the *Ch25h* gene were designed (Table S1) and their efficacy was evaluated (Figure 3A). siRNA-2 demonstrated optimum inhibition of CH25H at both the mRNA and protein levels (termed as *Ch25h*_si2), and was thus chosen for subsequent experiments. The optimal *Ch25h*_si2 was transfected into Raw264.7 cells which were then infected with WT_*Mm*. At 4 hpi, cells were harvested and stained for foam cells. Reduced foam cell formation after CH25H silencing was evident following WT_*Mm* challenge (Figures 3B and 3C). Interestingly, a mouse CH25H overexpression plasmid was constructed and termed CH25H_OE (Figures S3A and S3B) and its efficiency in Raw264.7 cells was evaluated (Figure 4A). CH25H_OE was transinfected into Raw264.7 macrophages and oil red O staining found numerous foam cells was formed even in ΔPDIM group after CH25H overexpression (Figures 4B and 4C). Consistently, the addition of 25HC, the enzymatic product of CH25H, into ΔPDIM-infected groups significantly promoted foam cell formation (Figures 4D and 4E). Taken together, our findings indicate that pathogenic mycobacteria induce foam cell formation and CH25H contributes to this process.

Pathogenic mycobacteria induce CH25H primarily via Toll-like receptor 4 (TLR4) signaling

Previous studies demonstrated that expression of CH25H was markedly upregulated in macrophages stimulated with a TLR4-related agonist, but not lipoteichoic acid (LTA), a TLR2 agonist.[37,38] In our study, we detected CH25H proteins in macrophages with a panel of activators and antagonists for TRL2 and TLR4, with or without WT- or ΔPDIM-*Mm* challenge. We found that the lower expression of CH25H in ΔPDIM-treated macrophages was significantly increased after exposure to LPS (Figures 5A and S4A). In contrast, CH25H was highly expressed in WT_*Mm*-infected macrophages but decreased dramatically after treatment with the TLR4 signaling inhibitor, TAK-242 (Figures 5B and S4B). However, neither LTA nor the TLR2 inhibitor, C29, impacted the expression trend of CH25H in macrophages following WT- or ΔPDIM-*Mm* infection (Figures 5C and S4C). Similarly, TAK-242 significantly reduced ADRP expression in WT_*Mm*-treated macrophages, while LPS enhanced ADRP in the ΔPDIM-infected group (Figures 5D, S4D, and S4E). Finally, oil red O staining demonstrated that LPS treatment rescued foam cell formation, resulting in increased foam cells in the LPS-treated ΔPDIM group (Figures 5E and 5F). Our results demonstrate that pathogenic mycobacteria promote foam cell formation by induction of CH25H expression via TLR4 signaling.

CH25H exacerbates morbidity in mice following mycobacterial infection

Next, we sought to determine the impact of CH25H on the outcome of mycobacterial infection *in vivo*. Genotyped *Ch25h*$^{-/-}$ mice (Figures S5A and S5B), and age- and sex-matched *Ch25h*$^{+/+}$ siblings were intravenously injected with the same number of WT- or ΔPDIM-*Mm*.[10] Surprisingly,

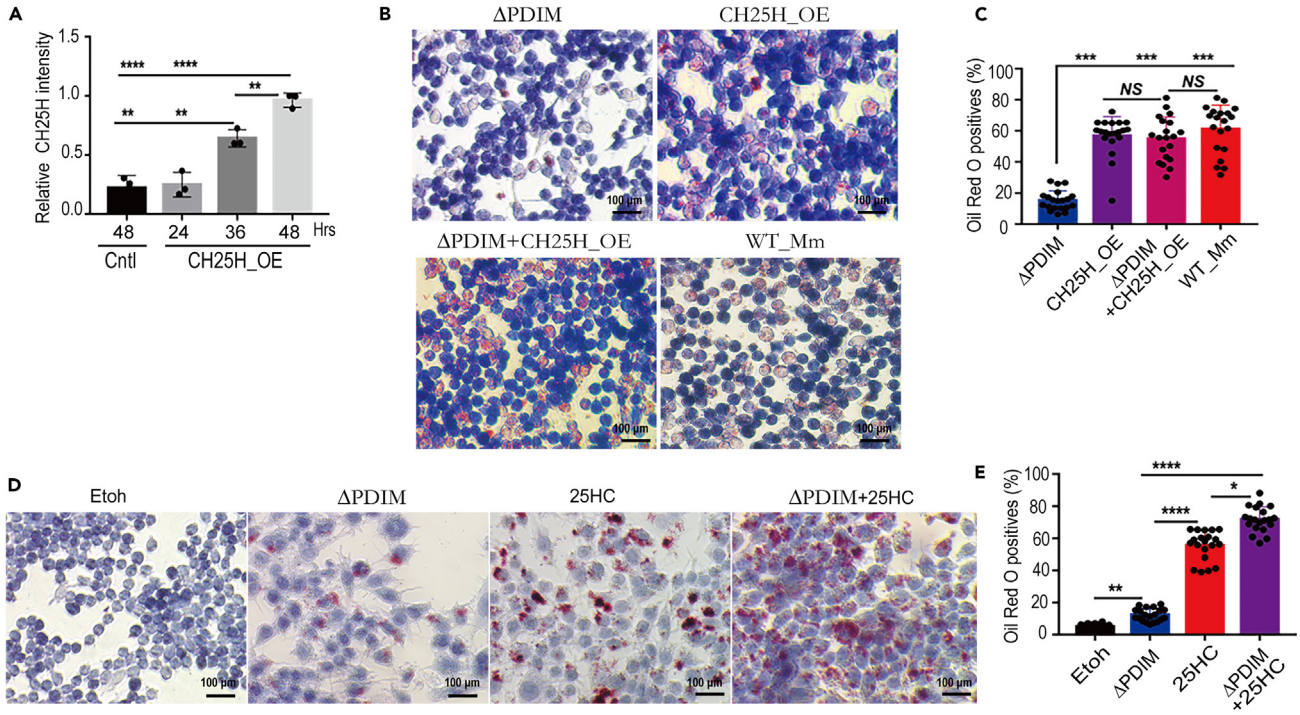

Figure 4. CH25H promotes the formation of foam cells

(A) CH25H protein level was enhanced after CH25H_OE was transfected into Raw264.7 macrophages and compared (**p < 0.01; ****p < 0.0001). Data are representative of three biologically independent experiments.

(B and C) CH25H_OE was transinfected into Raw264.7 and following infection with ΔPDIM_*Mm*, oil Red O staining found numerous foam cells were developed (***p < 0.001; *NS*, no significance). Data are representative of three biologically independent experiments.

(D and E) 25HC markedly promoted the foam cell formation, especially supplementation into attenuated ΔPDIM_*Mm*-challenged groups (*p < 0.05; **p < 0.01; ****p < 0.0001). Data are representative of three biologically independent experiments.

Ch25h$^{-/-}$ mice were relatively protected following WT_*Mm* infection and only scattered abscesses were formed, while *Ch25h*$^{+/+}$ counterparts demonstrated progressive larger-scale visible tail lesions (Figures 6A, S5C, and S5D). CFU counts demonstrated a decrease in the number of bacteria in WT_*Mm*-infected *Ch25h*$^{-/-}$ mice (Figure 6B). Histopathological evaluation revealed that there were numerous infiltrating inflammatory cells and granulomatous lesions in WT_*Mm*-infected *Ch25h*$^{+/+}$ mice, whereas fewer inflammatory cells were observed in their *Ch25h*$^{-/-}$ siblings (Figure 6C). ZN staining found red rod bacteria distributed in tissues from WT_*Mm*-infected *Ch25h*$^{+/+}$ and *Ch25h*$^{-/-}$ mice, but not in ΔPDIM-infected *Ch25h*$^{-/-}$ mice (Figure 6D). Oil red O staining showed that numerous foam cells were formed and extensively distributed in the granulomatous lesions of WT *Mm*-infected *Ch25h*$^{+/+}$ mice (Figures 6E and S6A), while decreased foam cells were observed in matched *Ch25h*$^{-/-}$ siblings (Figures 6E and S6B). Immunohistochemistry staining demonstrated that CH25H was highly expressed within granulomatous lesions (Figure 6F). Consistent with foam cell dynamics, ADRP was highly expressed in WT_*Mm*-infected *Ch25h*$^{+/+}$ mice, but not in their *Ch25h*$^{-/-}$ siblings (Figure 6G). Finally, CH25H and ADRP were also highly expressed in lung tissues from *Mtb*-challenged mice, rabbits, and marmosets as well as clinical tuberculosis patient specimens, distributed particularly within granulomas (Figures 7 and S7). Taken together, pathogenic mycobacteria could induce CH25H to aggravate the pathology and promote foam cell development during granuloma formation.

Atorvastatin mitigates mycobacteria-mediated pathology by reducing foam cell formation via inhibition of CH25H

Atorvastatin administration markedly decreased *in vitro* foam cell formation following WT_*Mm* infection of Raw264.7 cells (Figures 8A and S8), and accordingly, the mRNA levels of CH25H and ADRP were also reduced (Figures 8B and 8C). Notably, CH25H protein was also dramatically decreased in atorvastatin-treated macrophages infected with WT_*Mm* (Figures 8D and 8E). The mouse infection model demonstrated smaller lesions in both atorvastatin- and rifampicin-treated animals, whereas progressive inflammatory lesions formed in untreated mice (Figures 8F and S9). CFU counts identified decreased bacterial numbers in mice following either atorvastatin or rifampicin treatment (Figure 8G). Western blot demonstrated that CH25H expression was significantly decreased in both atorvastatin- and rifampicin-treated WT_*Mm*-infected mice (Figures 8H and 8I). Interestingly, ultrahistopathology inspection demonstrated tight apposition between *Mm*-containing phagosomes and host lipid bodies (Figure S10A), in particular, the bacilli-containing phagosomes showed a tendency to be engulfed by lipid bodies (Figures S10B and S10C). Our data indicate that CH25H may act as a critical player during statin-mediated adjuvant therapy against *Mtb*.

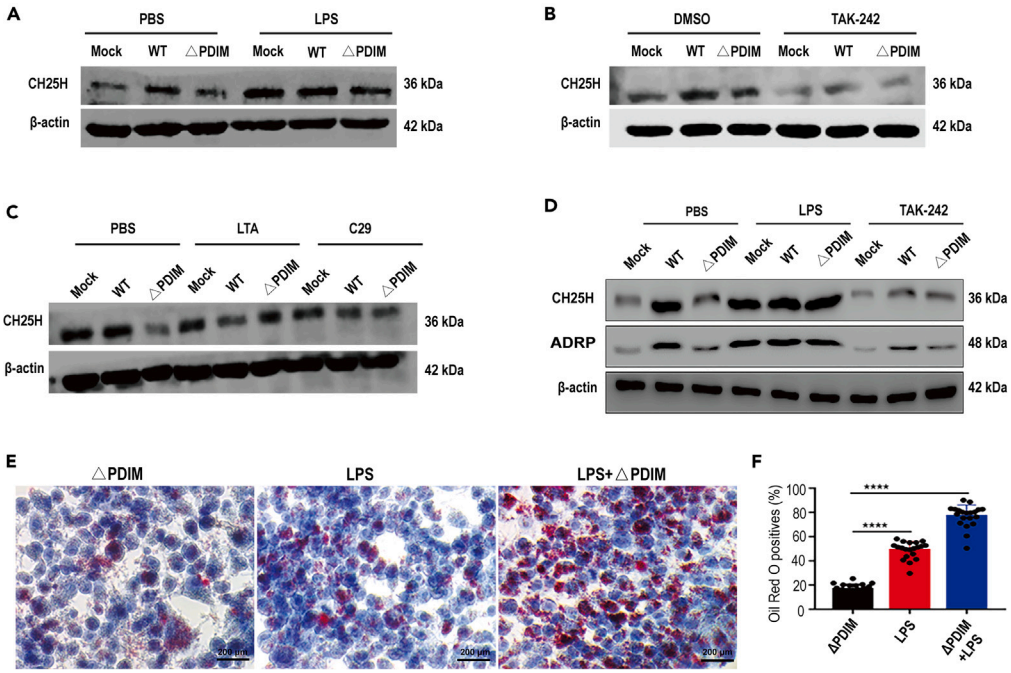

Figure 5. Pathogenic mycobacteria promote foam cell formation via upregulated CH25H through TLR4 signaling activation

(A) LPS, a specific TLR4 agonist, greatly induced the upregulation of CH25H in ΔPDIM-infected macrophages (LPS 10 ng/mL).

(B) TAK-242, an antagonist for the TLR4 signal, markedly reduced the CH25H production even under WT_*Mm* challenging (TAK-242: 100 nM).

(C) Either LTA (10 μg/mL) or C29 (100 μM), the specific activator and inhibitor for TLR2 signal, has no significant effects on the CH25H expression.

(D) Either LPS or TAK-242 remarkably changed the expression profile of CH25H and ADRP under WT_*Mm* and/or ΔPDIM strain inoculation.

(E) Oil red O stain demonstrated that numerous foam cells were formed under LPS treatment and LPS co-incubated ΔPDIM_*Mm* (40× magnification).

(F) Quantitation of oil red O cells demonstrated that the LPS supplement promotes the foam cell formation in the ΔPDIM-infected group (****$p < 0.0001$). Data are representative of three biologically independent experiments.

DISCUSSION

Macrophages are not only the first line of host defense against *Mtb*, but also the primary parasitic niche for mycobacteria. For defense against macrophage-mediated immunosurveillance and killing, pathogenic mycobacteria induce granuloma development to facilitate bacterial survival and dissemination.[7] Foam cells, originally described in atherosclerosis, are characterized by the formation of lipid-rich atheromatous lesions, which are not only thought to be a key driver of atherosclerotic diseases[15,16] but have also emerged as a crucial setting during mycobacteria-induced granuloma formation.[14,19,21,23,39–42] *Mtb* induces macrophage conversion into foam cells to reduce host cell capacity as well as make them a nutrient-rich reservoir for mycobacteria.[21,42] Although reports have demonstrated that foam cells play an important role in sustaining persistent bacteria and contributing to granuloma formation, the critical factor regulating the transdifferentiation of macrophages into foam cells remains unclear.

Recently, there was a report demonstrating that *Mtb*-infected cells upregulate the oxysterol-producing enzyme CH25H on the circulating eosinophils in both mice and rhesus macaque models, and highly expressed CH25H in infected murine alveolar macrophages could promote the pulmonary recruitment of eosinophils during the early exposure to *Mtb*.[43] In line with the CH25H upregulation in mice alveolar macrophages, our study demonstrated that CH25H is also upregulated in Raw264.7 macrophages and acts as an essential mediator for macrophage-derived foam cell formation during mycobacterial infection *in vivo* and *in vitro*. CH25H-*null* mice showed decreased foam cell formation and enhanced elimination of mycobacteria compared with *Ch25h*$^{+/+}$ siblings. Abundant foam cells were formed and distributed within granulomatous lesions in WT_*Mm*-infected *Ch25h*$^{+/+}$ mice, but not in *Ch25h*$^{-/-}$ siblings. Cumulative studies have demonstrated that CH25H and its enzymatic product, 25HC, act as a critical factor in modulating foam cell formation in a mouse model of diet-induced atherosclerosis.[16] Consistent with this, we found that CH25H promotes the transdifferentiation of Raw264.7 macrophages into foam cells. Moreover, we also found that increased foam cells developed in LPS-activated Raw264.7 macrophages, while specific inhibition of TLR4 signaling repressed foam cell formation even following *Mm* infection.

Atorvastatin, a statin family member, markedly repressed mycobacterial viability and improved tissue damage when combined with rifampicin.[44] Statin treatment markedly decreased the bacterial burden and reduced pathology in an *Mtb*-infected murine model.[24] Recent studies demonstrated that simvastatin not only enhances the immune response against *Mtb* by promoting apoptosis,[45] but also significantly strengthens the bactericidal activity of first-line drugs for tuberculosis in mice.[25] Although increasing reports in the literature have demonstrated that statins have direct and/or indirect anti-mycobacterial effects and could act as an adjuvant for tuberculosis treatment, the critical

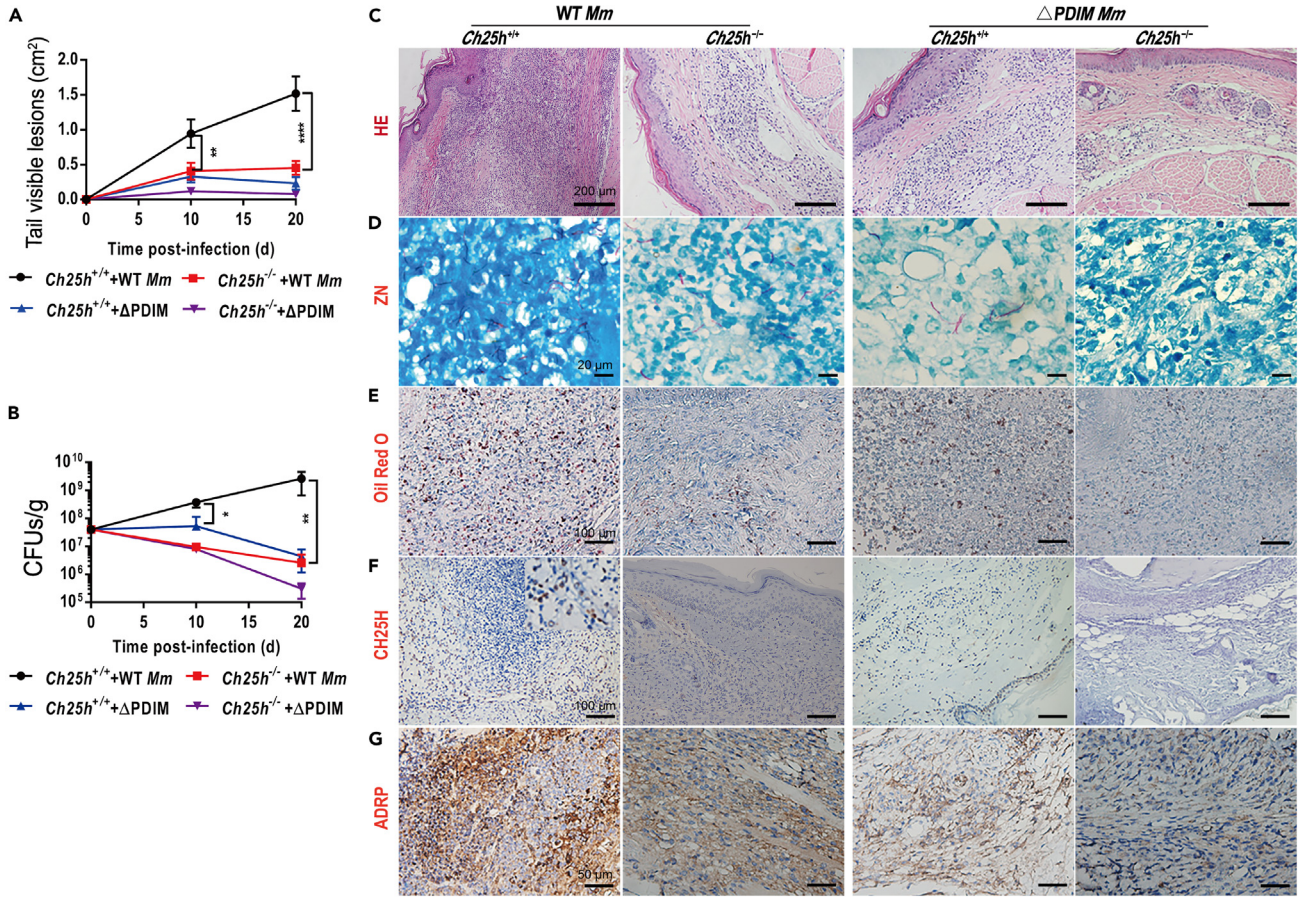

Figure 6. CH25H exacerbates pathology in mice after mycobacterial infection via promoting foam cell formation

(A) *Ch25h*$^{+/+}$ mice developed progressive and large inflammatory lesions compared to the reduced issues with their *Ch25h*$^{-/-}$ siblings after WT_*Mm* infection (n = 5).

(B) Host mycobacterial loading was gradually decreased in *Ch25h*$^{-/-}$ mice compared with the wide-type siblings after WT_*Mm* infection (n = 5).

(C) Histopathology examination demonstrated that typical granulomatous lesions formed in *Ch25h*$^{+/+}$ mice after WT_*Mm* infection (20× magnification).

(D) ZN staining for detecting the *mycobacterium marinum* in mice tissues (100× magnification).

(E) Oil red O combined with hematoxylin staining found that there were plentiful foam cells in WT_*Mm*-challenged *Ch25h*$^{+/+}$ mice, whereas the formation of foam cells markedly decreased in their *Ch25h*$^{-/-}$ siblings (32× magnification).

(F) Immunohistochemistry staining found that CH25H proteins were highly expressed and primarily distributed within granulomatous lesions (32× magnification).

(G) ADRP is obviously expressed in WT_*Mm*-challenged *Ch25h*$^{+/+}$ mice compared to their *Ch25h*$^{-/-}$ siblings and disseminated within the granulomatous lesions (40× magnification).

player during this process remains to be identified. Consistent with previous reports, we found that atorvastatin inhibited the expression of CH25H, thereby decreasing foam cell formation and improving pathology during mycobacterial infection. Our data imply that inhibiting foam cell development may be an unrecognized anti-tuberculosis mechanism of statins, and CH25H plays an important role during this process.

We compared gross lesions and histopathology between *Ch25h*$^{-/-}$ mice and their *Ch25h*$^{+/+}$ siblings after *Mm* infection at matched time-points. We found scattered small tail lesions and mild infiltration of inflammatory cells in *Ch25h*$^{-/-}$ mice, but progressive and granulomatous lesions in their *Ch25h*$^{+/+}$ siblings. CH25H-*null* mice also exhibited powerful antimicrobial activity and reduced pathology compared with the increasing bacterial loading in their *Ch25h*$^{+/+}$ siblings. These results are consistent with a previous report that CH25H-deficient mice showed a stronger capacity to repress *Listeria monocytogenes* growth *in vivo*.[31] Moreover, deletion of CH25H demonstrated a stronger protective effect in a mouse model of influenza infection due to decreased inflammatory pathology.[32] Our data suggest that in this murine infection model, *Mm* challenge upregulated CH25H to alter the inflammatory response, thereby amplifying inflammatory signaling.

In conclusion, to our knowledge, this study presents the first report of a previously unknown role of CH25H in modulating foam cell formation during mycobacterial infection, although further investigation of the detailed mechanism of mycobacterial regulation of CH25H expression and function remains necessary. Deletion of CH25H reduced the formation of foam cells and attenuated pathology in mice. CH25H also acts as an intrinsic effector linking statins and their anti-tuberculosis function. Thus, "host-directed therapy" targeting CH25H-mediated foam cell formation may lead to a more robust immune response against *Mtb*. Through this mechanism, the regulation of CH25H has the

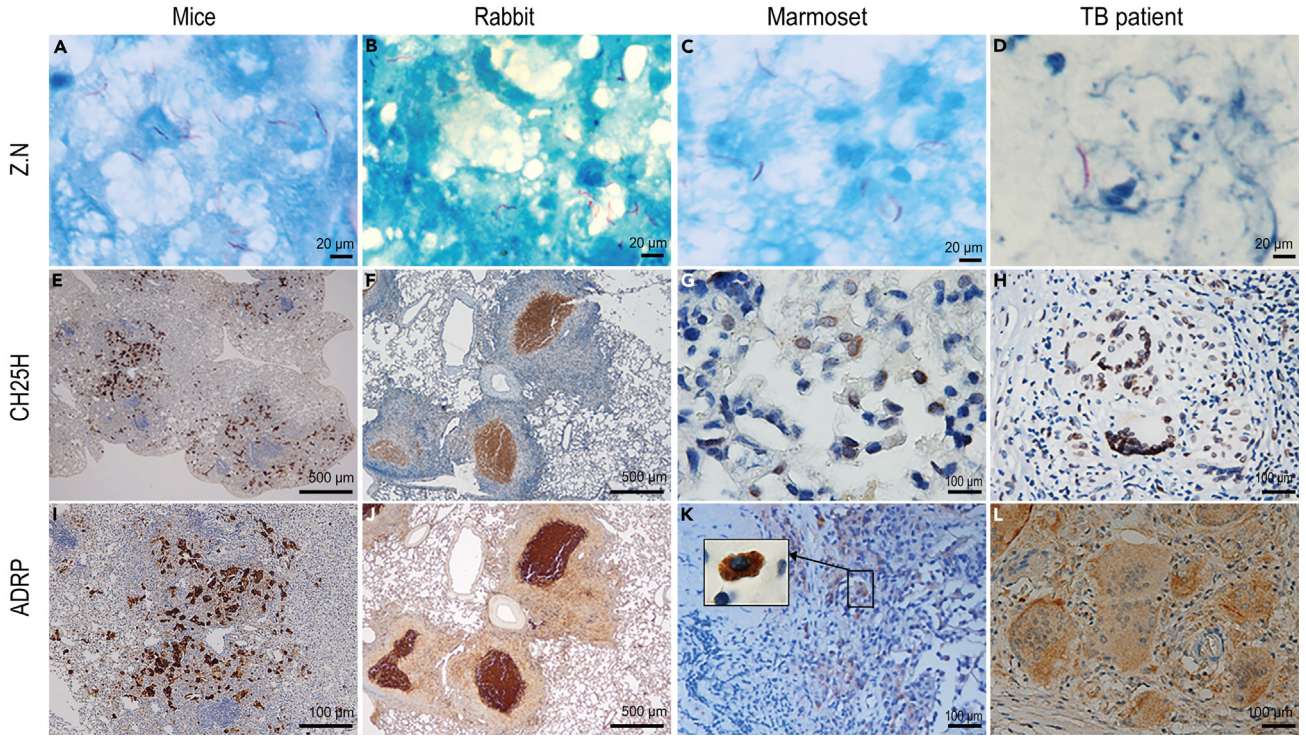

Figure 7. Profile of CH25H and ADRP in tissues from *Mtb*-challenged mice, rabbit and marmoset and clinical tuberculosis patient

(A–D) ZN staining showed that there were red-rod bacteria among different animal tissues including *Mtb*-infected lungs from mice, rabbits, and marmoset and clinical tuberculosis patients (100× magnification).

(E–H) CH25H is specifically expressed within the granulomatous lesions from *Mtb*-challenged mice, rabbit and marmoset, and TB patients ((E) and (F): 200× magnification; (G): 40× magnification; (H): 32× magnification).

(I–L) ADRP is expressed specifically within the granulomatous lesions of *Mtb*-challenged mice, rabbit and marmoset, and TB patients. In clinical TB patient samples, ADRP is markedly distributed within the multinuclear giant cells ((J): 200× magnification; (I), (K), and (L): 40× magnification).

potential to be a viable means to shorten the overall duration of tuberculosis chemotherapies. Strategies targeting CH25H activity can be used as adjuvant therapy against *Mtb* and may avoid the development of drug resistance, thereby being conducive to the prevention and control of tuberculosis.

Limitations of the study

Although the present study provides interesting information on the role of CH25H-mediated foam cells for the formation of granuloma during mycobacterial infection, there are still some limitations that should be clarified in future studies. For instance, although CH25H was markedly up-regulated during mycobacterial in our study as well as other reports,[29,43] considering the complex composition of mycobacteria and architecture of the mycobacteria cell wall and both structural and functional roles PDIM plays during infection,[34,46] PDIM may not be the sole molecular component necessary for the upregulation of CH25H. Other bacterial components, in the absence of PDIM, may not present to the host cell in the same way, also influencing the host response to infection, whether they share a similar axis for the CH25H induction during mycobacterial infection. Although CH25H functionally produces 25HC, CH25H and 25HC may have different functions and affect various pathophysiological processes, experiments to identify the details and the potential mechanism of 25HC for granuloma formation will provide a deeper perspective of oxysterols during mycobacterial infection. Furthermore, a recent study revealed that CH25H indeed affects the eosinophil recruitment at the earliest response to *Mtb*-infection,[43] and about the same time another report also demonstrated that some specific populations of eosinophils that expressed IL-4 and IL-13 within the granuloma,[47] so whether CH25H drive granuloma formation by regulating eosinophil's function and its interaction with macrophages during mycobacterial infection should be addressed in future studies.

STAR★METHODS

Detailed methods are provided in the online version of this paper and include the following:

- KEY RESOURCES TABLE
- RESOURCE AVAILABILITY

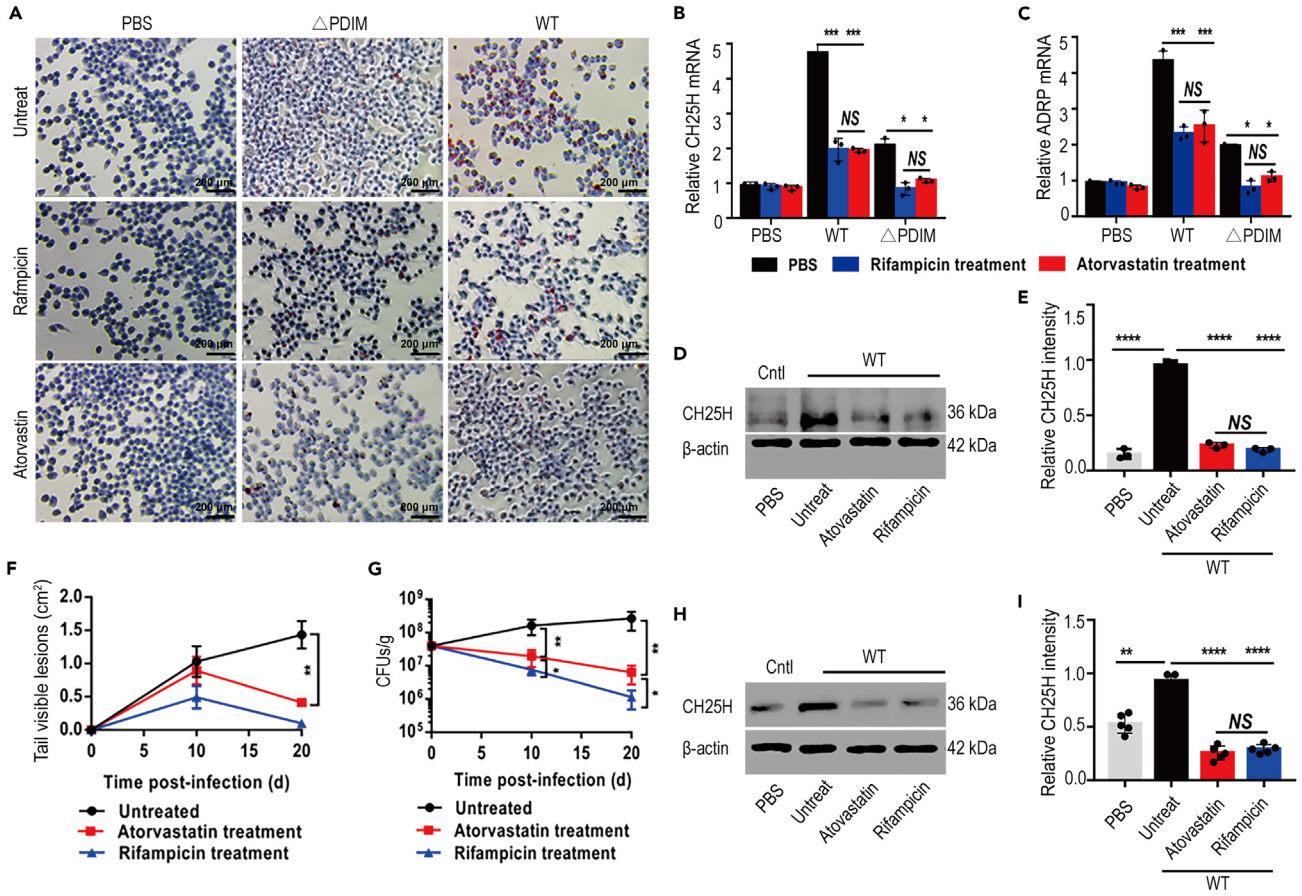

Figure 8. Atorvastatin administration decreased the CH25H expression and inhibited the formation of foam cells

(A) Atorvastatin administration inhibited the formation of foam cells even under WT_*Mm* infection (20× magnification).

(B and C) Atorvastatin treatment significantly reduced the mRNA expression level of CH25H and ADRP (*p < 0.05; ***p < 0.001). Data are representative of three biologically independent experiments.

(D and E) Atorvastatin treatment greatly decreased the protein level of CH25H in WT_*Mm*-infected cells (****p < 0.0001). Data are representative of three biologically independent experiments.

(F and G) Atorvastatin administration remitted the tissue damages under WT_*Mm* infection (*p < 0.05; **p < 0.01) (n = 5). Data are representative of three biologically independent experiments.

(H and I) Atorvastatin application dramatically reduced CH25H expression in WT_*Mm*-inoculated mice (**p < 0.01; ****p < 0.0001).

- Expression of CH25H and ADRP in granulomatous lesions from *Mtb*-infected animals and clinical tuberculosis patients
- Transmission electron microscopy (TEM)

- QUANTIFICATION AND STATISTICAL ANALYSIS

SUPPLEMENTAL INFORMATION

Supplemental information can be found online at https://doi.org/10.1016/j.isci.2024.109204.

ACKNOWLEDGMENTS

Decheng Wang is a special volunteer trainee of the Tuberculosis Research Section, LCIM, NIAID of National Institutes of Health. Material Analysis and Testing Center of China Three Gorges University provided the Confocal Microscope System. We thank Gillian Campbell, PhD, from Liwen Bianji, Edanz Group China (www.liwenbianji.cn/ac), for editing the English text of a draft of this manuscript. This work was supported in part by the National Natural Science Foundation of China (grant nos. 31772709 and 31572485 to D.W.; 82272353to L.Z.), and the Open Foundation of Hubei Province Key Laboratory of Tumor Microenvironment and Immunotherapy (no. 2023KZL017), the new faculty startup research fund of China Three Gorges University (KJ2014B023 to D.W.), and in part by the intramural research program of NIAID, NIH (Bethesda MD, USA). We would like to dedicate this paper to the memory of our beloved Dr. Weifeng Huang, who passed away during the preparation and writing of this manuscript.

AUTHOR CONTRIBUTIONS

S.Z., L.Z., and D.C.W. designed the project; S.Z., D.Z., D.L., H.K.W., C.R.D., J.R.S., W.F.H., X.X., Z.W.Z., S.S.H., Z.J., B.Y., J.G., L.E.V., L.Z., and D.C.W. performed the experiments; L.Z. and D.C.W. analyzed the data and wrote the draft; L.E.V. did the critical reading for the draft; L.E.V. and D.C.W. revised the manuscript; D.C.W. re-submitted the manuscript.

DECLARATION OF INTERESTS

The authors declare no competing interests.

Received: August 17, 2023
Revised: November 20, 2023
Accepted: February 7, 2024
Published: February 12, 2024

REFERENCES

1. Russell, D.G., Barry, C.E., 3rd, and Flynn, J.L. (2010). Tuberculosis: what we don't know can, and does, hurt us. Science (New York, N.Y.) *328*, 852–856. https://doi.org/10.1126/science.1184784.
2. Awuh, J.A., and Flo, T.H. (2017). Molecular basis of mycobacterial survival in macrophages. Cell. Mol. Life Sci. *74*, 1625–1648. https://doi.org/10.1007/s00018-016-2422-8.
3. Brennan, P.J., and Nikaido, H. (1995). The envelope of mycobacteria. Annu. Rev. Biochem. *64*, 29–63. https://doi.org/10.1146/annurev.bi.64.070195.000333.
4. Cox, J.S., Chen, B., McNeil, M., and Jacobs, W.R., Jr. (1999). Complex lipid determines tissue-specific replication of Mycobacterium tuberculosis in mice. Nature *402*, 79–83. https://doi.org/10.1038/47042.
5. Brennan, P.J. (2003). Structure, function, and biogenesis of the cell wall of Mycobacterium tuberculosis. Tuberculosis *83*, 91–97.
6. Tobin, D.M., and Ramakrishnan, L. (2008). Comparative pathogenesis of Mycobacterium marinum and Mycobacterium tuberculosis. Cell Microbiol. *10*, 1027–1039. https://doi.org/10.1111/j.1462-5822.2008.01133.x.
7. Davis, J.M., and Ramakrishnan, L. (2009). The role of the granuloma in expansion and dissemination of early tuberculous infection. Cell *136*, 37–49. https://doi.org/10.1016/j.cell.2008.11.014.
8. Oehlers, S.H., Cronan, M.R., Scott, N.R., Thomas, M.I., Okuda, K.S., Walton, E.M., Beerman, R.W., Crosier, P.S., and Tobin, D.M. (2015). Interception of host angiogenic signalling limits mycobacterial growth. Nature *517*, 612–615. https://doi.org/10.1038/nature13967.
9. Volkman, H.E., Pozos, T.C., Zheng, J., Davis, J.M., Rawls, J.F., and Ramakrishnan, L. (2010). Tuberculous granuloma induction via interaction of a bacterial secreted protein with host epithelium. Science (New York, N.Y.) *327*, 466–469. https://doi.org/10.1126/science.1179663.
10. Carlsson, F., Kim, J., Dumitru, C., Barck, K.H., Carano, R.A.D., Sun, M., Diehl, L., and Brown, E.J. (2010). Host-detrimental role of Esx-1-mediated inflammasome activation in mycobacterial infection. PLoS Pathog. *6*, e1000895. https://doi.org/10.1371/journal.ppat.1000895.
11. Ehlers, S., and Schaible, U.E. (2012). The granuloma in tuberculosis: dynamics of a host-pathogen collusion. Front. Immunol. *3*, 411. https://doi.org/10.3389/fimmu.2012.00411.
12. Ramakrishnan, L. (2012). Revisiting the role of the granuloma in tuberculosis. Nat. Rev. Immunol. *12*, 352–366. https://doi.org/10.1038/nri3211.
13. Rubin, E.J. (2009). The granuloma in tuberculosis–friend or foe? N. Engl. J. Med. *360*, 2471–2473. https://doi.org/10.1056/NEJMcibr0902539.
14. Russell, D.G., Cardona, P.J., Kim, M.J., Allain, S., and Altare, F. (2009). Foamy macrophages and the progression of the human tuberculosis granuloma. Nat. Immunol. *10*, 943–948. https://doi.org/10.1038/ni.1781.
15. Lundberg, B. (1985). Chemical composition and physical state of lipid deposits in atherosclerosis. Atherosclerosis *56*, 93–110.
16. Gold, E.S., Ramsey, S.A., Sartain, M.J., Selinummi, J., Podolsky, I., Rodriguez, D.J., Moritz, R.L., and Aderem, A. (2012). ATF3 protects against atherosclerosis by suppressing 25-hydroxycholesterol-induced lipid body formation. J. Exp. Med. *209*, 807–817. https://doi.org/10.1084/jem.20111202.
17. Almeida, P.E., Carneiro, A.B., Silva, A.R., and Bozza, P.T. (2012). PPARgamma Expression and Function in Mycobacterial Infection: Roles in Lipid Metabolism, Immunity, and Bacterial Killing. PPAR Res. *2012*, 383829. https://doi.org/10.1155/2012/383829.
18. Salamon, H., Bruiners, N., Lakehal, K., Shi, L., Ravi, J., Yamaguchi, K.D., Pine, R., and Gennaro, M.L. (2014). Cutting edge: Vitamin D regulates lipid metabolism in Mycobacterium tuberculosis infection. J. Immunol. *193*, 30–34. https://doi.org/10.4049/jimmunol.1400736.
19. Genoula, M., Marín Franco, J.L., Dupont, M., Kviatcovsky, D., Milillo, A., Schierloh, P.,

Moraña, E.J., Poggi, S., Palmero, D., Mata-Espinosa, D., et al. (2018). Formation of Foamy Macrophages by Tuberculous Pleural Effusions Is Triggered by the Interleukin-10/Signal Transducer and Activator of Transcription 3 Axis through ACAT Upregulation. Front. Immunol. *9*, 459. https://doi.org/10.3389/fimmu.2018.00459.

20. Shim, D., Kim, H., and Shin, S.J. (2020). Mycobacterium tuberculosis Infection-Driven Foamy Macrophages and Their Implications in Tuberculosis Control as Targets for Host-Directed Therapy. Front. Immunol. *11*, 910. https://doi.org/10.3389/fimmu.2020.00910.
21. Peyron, P., Vaubourgeix, J., Poquet, Y., Levillain, F., Botanch, C., Bardou, F., Daffé, M., Emile, J.F., Marchou, B., Cardona, P.J., et al. (2008). Foamy macrophages from tuberculous patients' granulomas constitute a nutrient-rich reservoir for M. tuberculosis persistence. PLoS Pathog. *4*, e1000204. https://doi.org/10.1371/journal.ppat.1000204.
22. Mahajan, S., Chandra, V., Dave, S., Nanduri, R., and Gupta, P. (2012). Stem bromelain-induced macrophage apoptosis and activation curtail Mycobacterium tuberculosis persistence. J. Infect. Dis. *206*, 366–376. https://doi.org/10.1093/infdis/jis354.
23. Johansen, M.D., Kasparian, J.A., Hortle, E., Britton, W.J., Purdie, A.C., and Oehlers, S.H. (2018). Mycobacterium marinum infection drives foam cell differentiation in zebrafish infection models. Dev. Comp. Immunol. *88*, 169–172. https://doi.org/10.1016/j.dci.2018.07.022.
24. Parihar, S.P., Guler, R., Khutlang, R., Lang, D.M., Hurdayal, R., Mhlanga, M.M., Suzuki, H., Marais, A.D., and Brombacher, F. (2014). Statin therapy reduces the mycobacterium tuberculosis burden in human macrophages and in mice by enhancing autophagy and phagosome maturation. J. Infect. Dis. *209*, 754–763. https://doi.org/10.1093/infdis/jit550.
25. Dutta, N.K., Bruiners, N., Pinn, M.L., Zimmerman, M.D., Prideaux, B., Dartois, V., Gennaro, M.L., and Karakousis, P.C. (2016). Statin adjunctive therapy shortens the duration of TB treatment in mice. J. Antimicrob. Chemother. *71*, 1570–1577. https://doi.org/10.1093/jac/dkw014.
26. Dutta, N.K., Bruiners, N., Zimmerman, M.D., Tan, S., Dartois, V., Gennaro, M.L., and Karakousis, P.C. (2020). Adjunctive Host-Directed Therapy With Statins Improves Tuberculosis-Related Outcomes in Mice. J. Infect. Dis. *221*, 1079–1087. https://doi.org/10.1093/infdis/jiz517.
27. Russell, D.W. (2003). The enzymes, regulation, and genetics of bile acid synthesis. Annu. Rev. Biochem. *72*, 137–174. https://doi.org/10.1146/annurev.biochem.72.121801.161712.
28. Liu, S.Y., Aliyari, R., Chikere, K., Li, G., Marsden, M.D., Smith, J.K., Pernet, O., Guo, H., Nusbaum, R., Zack, J.A., et al. (2013). Interferon-inducible cholesterol-25-hydroxylase broadly inhibits viral entry by production of 25-hydroxycholesterol. Immunity *38*, 92–105. https://doi.org/10.1016/j.immuni.2012.11.005.
29. Ngo, M.D., Bartlett, S., Bielefeldt-Ohmann, H., Foo, C.X., Sinha, R., Arachchige, B.J., Reed, S., Mandrup-Poulsen, T., Rosenkilde, M.M., and Ronacher, K. (2022). A Blunted GPR183/Oxysterol Axis During Dysglycemia Results in Delayed Recruitment of Macrophages to the Lung During Mycobacterium tuberculosis Infection. J. Infect. Dis. *225*, 2219–2228. https://doi.org/10.1093/infdis/jiac102.
30. Li, C., Deng, Y.Q., Wang, S., Ma, F., Aliyari, R., Huang, X.Y., Zhang, N.N., Watanabe, M., Dong, H.L., Liu, P., et al. (2017). 25-Hydroxycholesterol Protects Host against Zika Virus Infection and Its Associated Microcephaly in a Mouse Model. Immunity *46*, 446–456. https://doi.org/10.1016/j.immuni.2017.02.012.
31. Reboldi, A., Dang, E.V., McDonald, J.G., Liang, G., Russell, D.W., and Cyster, J.G. (2014). Inflammation. 25-Hydroxycholesterol suppresses interleukin-1-driven inflammation downstream of type I interferon. Science (New York, N.Y.) *345*, 679–684. https://doi.org/10.1126/science.1254790.
32. Gold, E.S., Diercks, A.H., Podolsky, I., Podyminogin, R.L., Askovich, P.S., Treuting, P.M., and Aderem, A. (2014). 25-Hydroxycholesterol acts as an amplifier of inflammatory signaling. Proc. Natl. Acad. Sci. USA *111*, 10666–10671. https://doi.org/10.1073/pnas.1404271111.
33. Li, Z., Martin, M., Zhang, J., Huang, H.Y., Bai, L., Zhang, J., Kang, J., He, M., Li, J., Maurya, M.R., et al. (2017). Krüppel-Like Factor 4 Regulation of Cholesterol-25-Hydroxylase and Liver X Receptor Mitigates Atherosclerosis Susceptibility. Circulation *136*, 1315–1330. https://doi.org/10.1161/circulationaha.117.027462.
34. Cambier, C.J., Takaki, K.K., Larson, R.P., Hernandez, R.E., Tobin, D.M., Urdahl, K.B., Cosma, C.L., and Ramakrishnan, L. (2014). Mycobacteria manipulate macrophage recruitment through coordinated use of membrane lipids. Nature *505*, 218–222. https://doi.org/10.1038/nature12799.
35. Wang, Q., Boshoff, H.I.M., Harrison, J.R., Ray, P.C., Green, S.R., Wyatt, P.G., and Barry, C.E., 3rd (2020). PE/PPE proteins mediate nutrient transport across the outer membrane of Mycobacterium tuberculosis. Science (New York, N.Y.) *367*, 1147–1151. https://doi.org/10.1126/science.aav5912.
36. Astarie-Dequeker, C., Le Guyader, L., Malaga, W., Seaphanh, F.K., Chalut, C., Lopez, A., and Guilhot, C. (2009). Phthiocerol dimycocerosates of M. tuberculosis participate in macrophage invasion by inducing changes in the organization of plasma membrane lipids. PLoS Pathog. *5*, e1000289. https://doi.org/10.1371/journal.ppat.1000289.
37. Bauman, D.R., Bitmansour, A.D., McDonald, J.G., Thompson, B.M., Liang, G., and Russell, D.W. (2009). 25-Hydroxycholesterol secreted by macrophages in response to Toll-like receptor activation suppresses immunoglobulin A production. Proc. Natl. Acad. Sci. USA *106*, 16764–16769. https://doi.org/10.1073/pnas.0909142106.
38. Diczfalusy, U., Olofsson, K.E., Carlsson, A.M., Gong, M., Golenbock, D.T., Rooyackers, O., Fläring, U., and Björkbacka, H. (2009). Marked upregulation of cholesterol 25-hydroxylase expression by lipopolysaccharide. J. Lipid Res. *50*, 2258–2264. https://doi.org/10.1194/jlr.M900107-JLR200.
39. Lovewell, R.R., Sassetti, C.M., and VanderVen, B.C. (2016). Chewing the fat: lipid metabolism and homeostasis during M. tuberculosis infection. Curr. Opin. Microbiol. *29*, 30–36. https://doi.org/10.1016/j.mib.2015.10.002.
40. Mahajan, S., Dkhar, H.K., Chandra, V., Dave, S., Nanduri, R., Janmeja, A.K., Agrewala, J.N., and Gupta, P. (2012). Mycobacterium tuberculosis modulates macrophage lipid-sensing nuclear receptors PPARγ and TR4 for survival. J. Immunol. *188*, 5593–5603. https://doi.org/10.4049/jimmunol.1103038.
41. Guerrini, V., Prideaux, B., Blanc, L., Bruiners, N., Arrigucci, R., Singh, S., Ho-Liang, H.P., Salamon, H., Chen, P.Y., Lakehal, K., et al. (2018). Storage lipid studies in tuberculosis reveal that foam cell biogenesis is disease-specific. PLoS Pathog. *14*, e1007223. https://doi.org/10.1371/journal.ppat.1007223.
42. Agarwal, P., Combes, T.W., Shojaee-Moradie, F., Fielding, B., Gordon, S., Mizrahi, V., and Martinez, F.O. (2020). Foam Cells Control Mycobacterium tuberculosis Infection. Front. Microbiol. *11*, 1394. https://doi.org/10.3389/fmicb.2020.01394.
43. Bohrer, A.C., Castro, E., Tocheny, C.E., Assmann, M., Schwarz, B., Bohrnsen, E., Makiya, M.A., Legrand, F., Hilligan, K.L., Baker, P.J., et al. (2022). Rapid GPR183-mediated recruitment of eosinophils to the lung after Mycobacterium tuberculosis infection. Cell Rep. *40*, 111144. https://doi.org/10.1016/j.celrep.2022.111144.
44. Lobato, L.S., Rosa, P.S., Ferreira, J.D.S., Neumann, A.D.S., da Silva, M.G., do Nascimento, D.C., Soares, C.T., Pedrini, S.C.B., Oliveira, D.S.L.D., Monteiro, C.P., et al. (2014). Statins increase rifampin mycobactericidal effect. Antimicrob. Agents Chemother. *58*, 5766–5774. https://doi.org/10.1128/AAC.01826-13.
45. Guerra-De-Blas, P.D.C., Bobadilla-Del-Valle, M., Sada-Ovalle, I., Estrada-García, I., Torres-González, P., López-Saavedra, A., Guzmán-Beltrán, S., Ponce-de-León, A., and Sifuentes-Osornio, J. (2019). Simvastatin Enhances the Immune Response Against Mycobacterium tuberculosis. Front. Microbiol. *10*, 2097. https://doi.org/10.3389/fmicb.2019.02097.
46. Cambier, C.J., Banik, S.M., Buonomo, J.A., and Bertozzi, C.R. (2020). Spreading of a mycobacterial cell-surface lipid into host epithelial membranes promotes infectivity. Elife *9*, e60648. https://doi.org/10.7554/eLife.60648.
47. Cronan, M.R., Hughes, E.J., Brewer, W.J., Viswanathan, G., Hunt, E.G., Singh, B., Mehra, S., Oehlers, S.H., Gregory, S.G., Kaushal, D., and Tobin, D.M. (2021). A non-canonical type 2 immune response coordinates tuberculous granuloma formation and epithelialization. Cell *184*, 1757–1774.e14. https://doi.org/10.1016/j.cell.2021.02.046.
48. Yu, J., Tran, V., Li, M., Huang, X., Niu, C., Wang, D., Zhu, J., Wang, J., Gao, Q., and Liu, J. (2012). Both phthiocerol dimycocerosates and phenolic glycolipids are required for virulence of Mycobacterium marinum. Infect. Immun. *80*, 1381–1389. https://doi.org/10.1128/IAI.06370-11.
49. Takaki, K., Davis, J.M., Winglee, K., and Ramakrishnan, L. (2013). Evaluation of the pathogenesis and treatment of Mycobacterium marinum infection in zebrafish. Nat. Protoc. *8*, 1114–1124. https://doi.org/10.1038/nprot.2013.068.
50. Wang, Y., Tang, Y., Lin, C., Zhang, J., Mai, J., Jiang, J., Gao, X., Li, Y., Zhao, G., Zhang, L., and Liu, J. (2022). Crosstalk between the ancestral type VII secretion system ESX-4 and other T7SS in Mycobacterium marinum. iScience *25*, 103585. https://doi.org/10.1016/j.isci.2021.103585.
51. Mehlem, A., Hagberg, C.E., Muhl, L., Eriksson, U., and Falkevall, A. (2013). Imaging of neutral lipids by oil red O for analyzing the metabolic status in health and disease. Nat.

Protoc. *8*, 1149–1154. https://doi.org/10.1038/nprot.2013.055.

52. Dai, L., DeFee, M.R., Cao, Y., Wen, J., Wen, X., Noverr, M.C., and Qin, Z. (2014). Lipoteichoic acid (LTA) and lipopolysaccharides (LPS) from periodontal pathogenic bacteria facilitate oncogenic herpesvirus infection within primary oral cells. PLoS One *9*, e101326. https://doi.org/10.1371/journal.pone.0101326.
53. Zhang, R., Tang, L., Tian, Y., Ji, X., Hu, Q., Zhou, B., Zhenyu, D., Heng, X., and Yang, L. (2020). Cholesterol-modified DP7 enhances the effect of individualized cancer immunotherapy based on neoantigens. Biomaterials *241*, 119852. https://doi.org/10.1016/j.biomaterials.2020.119852.
54. Xiao, L., Luo, G., Guo, X., Jiang, C., Zeng, H., Zhou, F., Li, Y., Yu, J., and Yao, P. (2020). Macrophage iron retention aggravates atherosclerosis: Evidence for the role of autocrine formation of hepcidin in plaque macrophages. Biochim. Biophys. Acta. Mol. Cell Biol. Lipids *1865*, 158531. https://doi.org/10.1016/j.bbalip.2019.158531.
55. Li, J., Lu, E., Yi, T., and Cyster, J.G. (2016). EBI2 augments Tfh cell fate by promoting interaction with IL-2-quenching dendritic cells. Nature *533*, 110–114. https://doi.org/10.1038/nature17947.
56. Song, J., Chao, J., Hu, X., Wen, X., Ding, C., Li, D., Zhang, D., Han, S., Yu, X., Yan, B., et al. (2022). E3 Ligase FBXW7 Facilitates Mycobacterium Immune Evasion by Modulating TNF-α Expression. Front. Cell. Infect. Microbiol. *12*, 851197. https://doi.org/10.3389/fcimb.2022.851197.
57. Parihar, S.P., Guler, R., Khutlang, R., Lang, D.M., Hurdayal, R., Mhlanga, M.M., Suzuki, H., Marais, A.D., and Brombacher, F. (2014). Statin therapy reduces the mycobacterium tuberculosis burden in human macrophages and in mice by enhancing autophagy and phagosome maturation. J. Infect. Dis. *209*, 754–763.
58. Via, L.E., Schimel, D., Weiner, D.M., Dartois, V., Dayao, E., Cai, Y., Yoon, Y.S., Dreher, M.R., Kastenmayer, R.J., Laymon, C.M., et al. (2012). Infection dynamics and response to chemotherapy in a rabbit model of tuberculosis using [^{18}F]2-fluoro-deoxy-D-glucose positron emission tomography and computed tomography. Antimicrob. Agents Chemother. *56*, 4391–4402. https://doi.org/10.1128/aac.00531-12.
59. Via, L.E., England, K., Weiner, D.M., Schimel, D., Zimmerman, M.D., Dayao, E., Chen, R.Y., Dodd, L.E., Richardson, M., Robbins, K.K., et al. (2015). A sterilizing tuberculosis treatment regimen is associated with faster clearance of bacteria in cavitary lesions in marmosets. Antimicrob. Agents Chemother. *59*, 4181–4189. https://doi.org/10.1128/aac.00115-15.

STAR★METHODS

KEY RESOURCES TABLE

REAGENT or RESOURCE	SOURCE	IDENTIFIER
Bacterial and virus strains		
Wide-type Mycobacterium marinum (WT_Mm)	Obtained from Qian Gao (Fudan University)	ATCC BAA-535
PDIM-deficient (ΔPDIM) Mycobacterium Marinum (ΔPDIM_Mm)		Infect Immun, 2012, 80, 1381–1389.
PDIM-deficient (ΔPDIM)_Complementary Mycobacterium marinum		Infect Immun, 2012, 80, 1381–1389.
tdTomato-labeled WT_Mm	This study	N/A
tdTomato-labeled ΔPDIM_Mm	This study	N/A
E.coli DH5α	Takara	Cat#9057
Antibodies		
CH25H antibody (AA 1–100) (IHC-P)	Antibody-Online	Cat#AA 1-100
Rabbit anti-ADRP	Abcam	Cat#ab108323; RRID:AB_10863476
Mouse ADRP Antibody	Santa Cruz Biotechnology	sc-390169
Mouse CH25H Antibody	Santa Cruz Biotechnology	sc-293256
Goat Anti-Rabbit IgG H&L (HRP)	Abcam	Cat#ab205718; RRID:AB_2819160
Goat Anti-Mouse IgG H&L (HRP)	Abcam	Cat#ab205719; RRID:AB_2755049
Rabbit anti-Actin	Abcam	Cat#ab179467; RRID:AB_2737344
Mouse anti-Actin	Abcam	Cat#ab8226; RRID:AB_306371
Chemicals, peptides, and recombinant proteins		
DMSO	Sigma-Aldrich	Cat#D8418
Mayer's Hematoxylin	Sigma-Aldrich	Cat#51275
25-hydroxycholesterol	Sigma-Aldrich	Cat#1015
LPS (lipopolysaccharides)	Sigma-Aldrich	Cat#0111:B4
C29	MedChem Express	HY-100461
TAK-242	MedChem Express	HY-11109
Lipoteichoic acid	Sigma-Aldrich	Cat#L3265
Glutaraldehyde	Sigma	Cat#354400
Critical commercial assays		
Middlebrook 7H9 Broth	BD-Difco	Cat#27131
Middlebrook 7H10 Broth	BD-Difco	Cat#262710
BD BBL Middlebrook OADC Enrichment	BD-Difco	Cat#211886
Hygromycin B	MedChemExpress	HY-B0490
Kanamycin	MedChemExpress	HY-16566
Ampicillin	MedChemExpress	HY-B0522
Gentamycin	MedChemExpress	HY-A0276A
Bodipy493/503	Sigma-Aldrich	Cat#790389
Dulbecco's modified Eagle medium	Gibco	Cat#12491015
Mouse CH25H (Cholesterol 25-hydroxylase) ELISA KIT	Cloud-Clone CORP	Cat#SEG357Mu
Mouse 25 Hydroxycholesterol (25OHC) ELISA kit	MyBioSource	Cat#MBS7256104
Dulbecco's phosphate-buffered saline	Sigma-Aldrich	Cat#D5773
0.5% Red Oil O stock	Sigma-Aldrich	Cat#O1391

(*Continued on next page*)

Continued

REAGENT or RESOURCE	SOURCE	IDENTIFIER
PrimeSTAR® GXL Premix	Takara	Cat#R050A
NotI	New England Biolabs	Cat#R0189S
SalI	New England Biolabs	Cat#R0138S
In-Fusion	Takara	Cat#638947
Lipomaster 2000 Transfection Reagent	Vazyme	Cat#TL201-01
Triton X-100	Sigma-Aldrich	Cat#T8787
Atorvastatin	MedChemExpress	Cat#HY-B0589
Rifampicin	MedChemExpress	Cat#HY-B0272
5-μm Filter	Pall	Cat#28144-095
Ethanol absolute	Sinopharm	Cat#100092008
BCA Protein Assay Kit	Beyotime Biotechnology	Cat#P0010S
Trizol	Invitrogen	Cat#15596018
SYBR qPCR Master Mix	Vazyme Biotech,	Cat#Q712-02
Experimental models: Cell lines		
Raw264.7 macrophages	This study	ATCC TIB71
Experimental models: Organisms/strains		
Ch25h−/− mice	Jackson Laboratories	JAX: 16263
Oligonucleotides		
Primers are listed in Table S1	This paper	N/A
Ch25h−/− mice genotyping primer	This paper	N/A
Ch25h_siRNA targeting Mouse *Ch25h* gene	This paper	N/A
Recombinant DNA		
MSCV-IRES-Thy1.1 DEST	Addgene	Plasmid #17442
Software and algorithms		
GraphPad Prism 4.0	Graphpad	https://www.graphpad.com
NIS-Elements Viewer	NIKON	www.microscope.healthcare.nikon.com/
Other		
Phosphate Buffer Saline	Solarbio Life Science	Cat#P1022
Bovine Serum Albumin	Solarbio Life Science	Cat#A8010
LB agar (powder)	Solarbio Life Science	Cat#L1015

RESOURCE AVAILABILITY

Lead contact

Further information and requests for resources and reagents should be directed to and will be fulfilled by the lead contact, Decheng Wang (dcwang99@163.com).

Materials availability

All unique/stable reagents generated in this study are available from the lead contact with a completed Materials Transfer Agreement.

Data and code availability

- Data reported in this paper will be shared by the lead contact upon request.
- This study did not generate any unique datasets or code.
- Any additional information required to reanalyze the data reported in this paper is available from the lead contact upon request.

METHOD DETAILS

Bacterial strains and growth conditions

Mycobacterium marinum (*Mm*) M strain (ATCC BAA-535) was used as the wild-type (WT) strain for this study,[48] and a PDIM-deficient (ΔPDIM) strain derived from a fadD26 mutation was used as an attenuated control.[48] All bacterial strains were grown at 32°C in 7H9 broth (Difco) supplemented with 10% oleic acid albumin dextrose-catalase (OADC enrichment), 0.5% glycerol, and 0.05% Tween 80 or on 7H10 agar with 10% OADC-0.5% glycerol. For fluorescence-labeled strains, 100 μL of 50 mg/mL hygromycin was added to 7H9-OADC per 100 mL.

Single-cell preparation of *mm* inocula

Briefly, the procedure of single-cell preparation of *Mm* inocula followed the established protocol.[49] Firstly, the WT_*Mm* and ΔPDIM_*Mm* strains were cultured at 32°C for about 7 days until the OD600 reached 0.5–0.8 respectively, and then harvested by centrifugation for 15 min at 4000 g at room temperature. Discarded the supernatant and resuspended the pellet with 1 mL 7H9-OADC. After well mixed, the 1 mL resuspension was aliquoted to 200 μL into and transferred into five 1.5 mL microcentrifuge tubes, then each aliquoted solution was aspirated and ejected ten times by using a 27-gauge syringe. Add 1mL 7H9-OADC to each 200 μL aliquot and mix each aliquot gently. After centrifugation, the supernatant was collected and passed through a sterile 5-μm filter to obtain single-cell bacteria. The final bacterial concentration was measured by plating serial dilutions onto 7H10-OADC plate and CFU counting after 7–10 days of incubation at 32°C. 5 mL aliquots of WT_*Mm* and/or ΔPDIM_*Mm* were stored at −80°C. Before proceeding with the infection experiments, the CFU were assessed from aliquots frozen at −80°C and the exact number of viable bacteria by plate it onto 7H10-OADC for enumeration of CFU.

Raw264.7 macrophage infection with *mm*

The murine macrophage line Raw264.7 was seeded into six-well plates at a density of 5×10^5 cells/well and maintained at 37°C in 5% CO_2 in Dulbecco's modified Eagle medium (DMEM) supplemented with 10% fetal bovine serum for 24 h before infection. Then macrophages were infected with WT_*Mm* and ΔPDIM_*Mm* at an indicated multiplicity of infection (MOI) of 5 at 32°C for 3 h in 5% CO_2. Cells were then gently washed three times with sterilized 1 × PBS buffer and incubated at 32°C in 5% CO_2 for 1 h with fresh medium containing 1 mg/mL gentamycin to kill extracellular bacilli. Then cells were washed twice with PBS and continuously incubated at 32°C in 5% CO_2 in fresh media with 20 μg/mL gentamycin. At different time points, the infected macrophage was collected and washed 3 times with PBS and the number of intracellular mycobacteria was confirmed by colony counting on 7H10-OADC plates according to an established protocol.[50]

Foam cell staining

Raw264.7 macrophages were infected with WT_*Mm* or ΔPDIM_*Mm*, with oxidized low-density lipoprotein (ox-LDL)-treatment as a positive control. Cells were harvested at 1, 4, 8 h post-infection (hpi) and washed twice with PBS. Remove PBS completely and fixed with 4% paraformaldehyde solution for 10 min at room temperature. Discard paraformaldehyde and add 3 mL fresh paraformaldehyde solution and then incubate for at least 1 h, or longer (cell sample can be kept in fixative for a couple of days before staining. Wrap with parafilm and cover with aluminum foil to prevent cells drying). Gently remove the paraformaldehyde solution with a pipette and wash the cells twice with ddH_2O. Continuously washed the cells with 60% isopropanol at room temperature. Completely remove the isopropanol and add 3mL Oil Red O working solution (mix 60mL 0.5% oil red O stock with 40 mL ddH_2O for 20 min and then filter) and incubate for 20 min. Rinsing cells immediately with ddH_2O and then counterstained with Mayer's Hematoxylin for 3 min. Wash cells three times with ddH_2O and acquire the images under the microscope. For tissue oil red O staining, the mouse tail was sectioned and stained according to a published protocol.[51]

Western blot

Raw264.7 was seeded into six-well plates at a density of 5×10^5 cells/well and then infected with WT or ΔPDIM *Mm* as described above. The infected macrophages were harvested at indicated time-points and protein was extracted. Protein concentration was assessed by using the BCA Protein Assay Kit, according to the manufacturer's instructions. Equal amounts of proteins were separated by SDS-PAGE and transferred to a nitrocellulose membrane. Nitrocellulose membranes were blocked in 5% bovine serum albumin (BSA) and subsequently probed with anti-CH25H (1:100, Santa Cruz Biotechnology, sc-293256) and anti-ADRP (1:1000, Abcam, ab108323) antibodies overnight. Indicated secondary antibodies conjugated to horseradish peroxidase were added, followed by visualization by using a ChemiQ system for imaging and analyzing gels. The results were confirmed by at least three independent experiments.

ELISA assay

Raw264.7 cells were seeded into six-well plates at a density of 5×10^5 cells/well and then infected with WT_*Mm* or ΔPDIM as described above. The cells of different groups at indicated time-points were collected and centrifuged for 15 min at 1000 g to remove cell debris and supernatants were harvested and performed different pre-processing according to exact detection objects including CH25H and 25HC. The contents of CH25H in the supernatant were measured immediately by using a commercial ELISA kit (Cloud-Clone CORP, China) according to the manufacturer's instructions. 25HC contents were detected by using a Mouse 25 Hydroxycholesterol (25OHC) ELISA kit (MyBioSource, MBS7256104). Each sample was dispensed in triplicate, and the optical density of each well was determined at 450 nm in a microplate reader. This study was performed independently 3 times on different groups in triplicates.

Confocal microscopy

Raw264.7 macrophages were seeded on glass coverslips in six-well plates and infected with WT- or ΔPDIM-*Mm*. At 4 hpi, cells were washed with PBS and fixed in 4% paraformaldehyde for 30 min, followed by incubation with BODIPY 493/503 (Sigma Sku790389) for 30 min in the dark. After washing with PBS, coverslips were observed under confocal microscopy (Nikon AIR, Japan). For lipid-droplet quantitation, 40 fields of each coverslip were imaged by using confocal microscopy (1× zoom, 5–6 cells/field). A total of 200 cells were captured and BODIPY 493/503-positives in stacked confocal micrographs of each group were calculated. For ADRP examination, cells were permeabilized with 0.1% Triton X-100, washed thrice with PBS and incubated with 1:500 diluted anti-ADRP antibody (ab108323) at 4°C overnight. Cells were again washed thrice with PBS, incubated with optimally diluted secondary antibody for 1 h, washed thrice with PBS and then counterstained with DAPI for 5 min. After washing, micrographs of ADRP were acquired by confocal microscopy.

Effects of CH25H silencing and/or overexpression on foam cell formation

To further demonstrate the role of CH25H in modulating foam cell formation, three specific small interfering RNA (siRNA) (termed *Ch25h_si1*, *Ch25_si2* and *Ch25h_si3*) against mouse *Ch25h* gene were designed, synthesized (Table S1) and their efficacy was evaluated in both mRNA and protein levels, and *Ch25_si2* has the optimum efficiency for CH25H inhibition in both mRNA and protein levels. Subsequently, the *Ch25_si2* was chosen for the continuous study to observe the effect of silencing CH25H on foam cell formation. On the contrary, a mouse *Ch25h* overexpression plasmid was constructed based on the backbone of MSCV-IRES-Thy1.1, then sequenced and finally termed as CH25H_OE. The CH25H_OE was transinfected into Raw264.7 macrophages and then infected with ΔPDIM_*Mm* at MOI = 5. At 8 hpi, all cells were harvested and stained with oil red O working solution as described above. Finally, 25HC—the major enzymatic product of CH25H, was dissolved with Etoh and administrated to detect the foam cell dynamics according to the published protocol.[30]

Raw264.7 macrophages treatment with TLR4 agonist LPS or antagonist TAK-242

To examine the induction of CH25H triggered from toll-like receptor 2 and/or 4 (TLR2/TLR4), Raw264.7 was seeded into six-well plates at a density of 5×10^5 cells/well and cultured. At the indicated time-points, the cells treated with TLR2 agonists lipoteichoic acid (LTA, Sigma)[52] or agonist C29 (MedChem Express, HY-100461),[53] or incubated with TLR4 agonist LPS (10 ng/mL) or antagonist TAK-242 (100 nM) as previously described.[54]

Generation of *Ch25h*$^{-/-}$ mice

Ch25h heterozygote mice (*Ch25h*$^{+/-}$) generated on the C57BL/6 background were kindly provided by Dr. Li (Fudan University).[55] Wide-type (WT) C57BL/6 mice were originally obtained from Shanghai SLAC Laboratory Animal Center and continuously bred in the Laboratory Animal Center of China Three Gorges University. *Ch25h*$^{+/-}$ mice were mated with WT C57BL/6 mice to generate more *Ch25h*$^{+/-}$ mice. WT (+/+) and homozygote (−/−) mice were obtained by intercrossing heterozygote (+/−) mice. The newborn mice were numbered and caged separately at 21 days, then a tail tip clipping of each mouse was obtained and treated with an animal genomic-DNA quick extraction kit (Beyotime Biotech) for DNA extraction. Finally, *Ch25h* homozygote (−/−) mice were identified and housed separately for use in subsequent experiments. All mice were housed in an SPF animal facility and provided with food and water *ad libitum*. The care and use of experimental animals complied with local animal welfare laws, guidelines, and policies. *Ch25h* homozygote (−/−) mice genotyping primer list as Table S2.

Infection of mice and harvesting of tails

Bacteria were cultured in 7H9 broth and harvested at the logarithmic growth phase (OD_{600} = 0.8–1.0) by centrifugation (1660×g, 10 min), and the final bacterial concentration was determined using a hemocytometer. Suspensions were diluted to 5×10^8 bacteria/mL. Female *Ch25h*$^{+/+}$ mice and *Ch25h*$^{-/-}$ mice, 30 of each, aged 8–10 weeks, were housed under SPF conditions (five mice/cage) in the Laboratory Animal Center of China Three Gorges University. Mice were anesthetized by isoflurane and injected intravenously with indicated WT or ΔPDIM *Mm* in 100 μL of sterile PBS as previously described.[10,56] At indicated time-points, five mice from each group were humanely euthanized. Tails were cut into 5 mm pieces, ground with a mortar and homogenized in 3 mL DMEM supplemented with 0.1% Triton X-. Tail suspensions were serially diluted and plated on 7H10 plates at 32°C and bacterial number was displayed as colony forming units (CFU)/g of tissue.[10] For monitoring visible tail lesions, the length and width of individual visible lesions were measured at indicated time-points and the lesions areas were calculated.[10] At day 10 and 20 post-infection, five mice from each group were sacrificed and tails were harvested and fixed with 4% paraformaldehyde for histopathology and immunohistochemical examination. The animal experiments were reviewed and approved by the Animal Care and Use Committee of China Three Gorges University (2019010I).

*q*RT-PCR

Samples from the different groups were harvested and immediately stored in a pre-cooled Trizol solution (Invitrogen, Cat#15596018). Total RNA was extracted by using a Trizol reagent according to the manufacturer's instructions. Then RNA was reverse transcribed to cDNA using the PrimeScript RT reagent Kit with gDNA Eraser (Takara, RR047A). Subsequently, the quantitative real-time PCR was performed by using the indicated primers for target genes including *Ch25h* (F: 5′-CCAGCTCCTAAGTCACGTC-3′; R: 5′-CACGTCGAAGAAGGTCAG-3′), and Adrp (F: 5′-AGTATCCCTACCTGAAGTCTGTG-3′; R: 5′-CCCCTTACAGGCATAGGTATTG-3′). The *Gapdh* (F: 5′-AGTGTTTCCTCGTCCCGTAG-3′; R: 5′-GCCGTGAGTGGAGTCATACT-3′) (Table S3) was used as an internal control and reference gene. The *q*RT-PCR was performed in

duplicate by using a StepOnePlus real-time PCR system (Applied Biosystems) and SYBR *q*PCR Master Mix (Vazyme Biotech, Cat#Q712-02). Fold changes were calculated by the $2^{-\Delta\Delta Ct}$ quantification method and related to reference gene expression values.

Atorvastatin intervention

In vitro intervention

Raw264.7 cells were cultured and pretreated with atorvastatin (5 μmol/L) for 2 h, then inoculated with WT or ΔPDIM *Mm*. Rifampicin (5 μg/mL) treatment was used as a positive control. After 4 h infection, cells were harvested and subjected to oil red O staining, CH25H and ADRP detection.

In vivo intervention

Female C57BL/6 mice (6–8 weeks old), were purchased from the Laboratory Animal Center of China Three Gorges University and inoculated intravenously with WT_*Mm* in 100 μL of sterile PBS, then randomly divided into three groups: control (untreated), rifampicin-treated (10 mg/kg body. weight) and atorvastatin-treated (20 mg/kg body.weight) groups.[57] At day 5 after WT_*Mm*-infection, rifampicin or atorvastatin were intraperitoneally injected every 2 days at the indicated dosage.

Expression of CH25H and ADRP in granulomatous lesions from *Mtb*-infected animals and clinical tuberculosis patients

Expression of CH25H and ADRP were detected in *Mtb*-infected mice, rabbits, marmosets, and clinical tuberculosis patients. The paraffin-embedded lung tissues of *Mtb* aerosol-infected mice, rabbits, and marmosets (under protocols LCIM-3, LCIM-4, and LCIM9) were obtained from the Tuberculosis Research Section of the National Institute of Allergy and Infectious Diseases, National Institutes of Health, Bethesda, MD.[58,59] Paraffin-embedded clinical tuberculosis patient samples were provided by the Third People's Hospital of Yichang and approved by the Ethics Committee of the Third People's Hospital of Yichang. Five-micrometer serial sections were made from all tissues and stained with Ziehl-Neelsen (Z.N), anti-CH25H and anti-ADRP antibodies, and images were captured by using the Cellsens imaging system (Olympus Life Sciences).

Transmission electron microscopy (TEM)

Tail tissue from WT_*Mm*-infected mice was collected and altered to small enough (about 3 mm in diameter) and immediately fixed with 2.5% glutaraldehyde solution for 3 h at 4°C. After rinsed with 0.1M phosphate buffer and post-fixed in 1% osmium tetroxide for 1 h. Subsequently, the tail tissues were dehydrated, embedded in epoxy resin, sectioned at 70 nm, and then performed staining with 2% uranyl acetate and 1% lead citrate. Finally, the ultrastructure of tail tissues especially the Mm-containing phagosomes and lipid bodies was inspected by using a Hitachi H-7500 transmission electron microscope (Hitachi Ltd., Tokyo, Japan).

QUANTIFICATION AND STATISTICAL ANALYSIS

All data are represented as mean ± standard deviation (SD) as indicated in the corresponding figure legends. Statistical analysis was performed with GraphPad Prism 4.0 (GraphPad Software, Inc., CA). All data are presented as the mean ± SD of at least 3 replicate analyses. For the comparison of two independent datasets, the Student's *t*-tests were applied and $p < 0.05$ was considered statistically significant. For more than two samples, statistical significance was determined by one-way ANOVA or two-way ANOVA followed test with a statistical threshold of $p < 0.05$.